Received: 27 October 2022 | Revised: 4 January 2023 | Accepted: 12 January 2023

DOI: 10.1111/mec.16849

ORIGINAL ARTICLE

MOLECULAR ECOLOGY WILEY

Integrating top-down and bottom-up approaches to understand the genetic architecture of speciation across a monkeyflower hybrid zone

Sean Stankowski | Madeline A. Chase | Hanna McIntosh | Matthew A. Streisfeld

Institute of Ecology and Evolution, University of Oregon, Eugene, Oregon, USA

Correspondence
Matthew A. Streisfeld, Institute of Ecology and Evolution, 5289 University of Oregon, Eugene, OR 97403, USA.
Email: mstreis@uoregon.edu

Present address
Sean Stankowski, IST Austria, AM1 Campus, Klosterneuburg, Austria

Madeline A. Chase, Department of Evolutionary Biology, Evolutionary Biology Centre (EBC), Uppsala University, Uppsala, Sweden

Hanna McIntosh, Department of Entomology, University of Wisconsin—Madison, Madison, Wisconsin, USA

Funding information
National Science Foundation, Grant/Award Number: DEB-1258199

Handling Editor: Richard J Abbott

Abstract

Understanding the phenotypic and genetic architecture of reproductive isolation is a long-standing goal of speciation research. In several systems, large-effect loci contributing to barrier phenotypes have been characterized, but such causal connections are rarely known for more complex genetic architectures. In this study, we combine "top-down" and "bottom-up" approaches with demographic modelling toward an integrated understanding of speciation across a monkeyflower hybrid zone. Previous work suggests that pollinator visitation acts as a primary barrier to gene flow between two divergent red- and yellow-flowered ecotypes of *Mimulus aurantiacus*. Several candidate isolating traits and anonymous single nucleotide polymorphism loci under divergent selection have been identified, but their genomic positions remain unknown. Here, we report findings from demographic analyses that indicate this hybrid zone formed by secondary contact, but that subsequent gene flow was restricted by widespread barrier loci across the genome. Using a novel, geographic cline-based genome scan, we demonstrate that candidate barrier loci are broadly distributed across the genome, rather than mapping to one or a few "islands of speciation." Quantitative trait locus (QTL) mapping reveals that most floral traits are highly polygenic, with little evidence that QTL colocalize, indicating that most traits are genetically independent. Finally, we find little evidence that QTL and candidate barrier loci overlap, suggesting that some loci contribute to other forms of reproductive isolation. Our findings highlight the challenges of understanding the genetic architecture of reproductive isolation and reveal that barriers to gene flow other than pollinator isolation may play an important role in this system.

KEYWORDS
barrier loci, barrier traits, cline, ecotypes, *Mimulus*, quantitative trait locus (QTL), reproductive isolation

1 | INTRODUCTION

Understanding the phenotypic and genetic architecture of reproductive isolation is a major goal of modern speciation research (Nosil, 2012; Ravinet et al., 2017; Seehausen et al., 2014). Early studies took a "top-down" approach by using quantitative trait locus (QTL) mapping and other association methods to detect genomic regions controlling barrier phenotypes or genetic incompatibilities (Fishman & Willis, 2001; Orr, 2001; Schemske & Bradshaw, 1999). More recently, "bottom-up" approaches, such as genome scans of

genomic differentiation (e.g., F_{ST}) or admixture (e.g., f_d), have identified candidate barrier loci in numerous systems, including those where isolation is thought to result from ecologically based divergent selection or intrinsic incompatibilities (Lamichhaney et al., 2015; Martin et al., 2013; Soria-Carrasco et al., 2014; Turner et al., 2005; Wang et al., 2022).

Although both approaches have clear strengths, they also present significant challenges (Barrett & Hoekstra, 2012). Top-down methods require that traits involved in reproductive isolation have already been identified, so our understanding of the genetic architecture of speciation can only ever be as complete as our knowledge of the traits controlling reproductive isolation in the system. In contrast, bottom-up approaches can provide a comprehensive view of the genomic landscape of speciation without complete knowledge of the isolating traits (but see Noor & Bennett, 2009; Cruickshank & Hahn, 2014; Ravinet et al., 2017). However, even though candidate barrier loci can be identified, their causal relationship with previously identified barrier traits usually remains unclear. This is because speciation usually involves many different isolating barriers (e.g., pre- and postzygotic, extrinsic and intrinsic) (Coyne & Orr, 2004; Stankowski & Ravinet, 2021) that can become coupled together through different aspects of the speciation process (Bierne et al., 2011;Butlin & Smadja, 2018 ; Smadja & Butlin, 2011). Although the coupling of different barriers eases speciation by generating a stronger overall barrier (Butlin & Smadja, 2018; Smadja & Butlin, 2011), the resulting linkage disequilibrium (LD) among barrier loci makes it difficult to understand their individual contributions to barrier traits. For example, a barrier locus identified in a genome scan might underlie an obvious phenotypic difference, or it may underlie a completely different barrier that is less conspicuous or that has yet to be discovered.

Therefore, instead of relying on one approach, many researchers have advocated for the integration of top-down and bottom-up methods (Barrett & Hoekstra, 2012; Faria et al., 2021; Ravinet et al., 2017). However, this kind of integration is missing from most studies of speciation. Although examples exist that show clear connections between large-effect loci underlying a barrier phenotype and signatures of selection (i.e., wing patterning in *Heliconius* butterflies: Martin et al., 2013), few attempts have been made to test for these associations when more complex genetic architectures contribute to reproductive isolation. This means that links between candidate barrier traits and barrier loci often remain tentative. To date, some of the best efforts to integrate top-down and bottom-up analyses have made use of natural hybrid zones between divergent populations (Abbott et al., 2013). Hybrid zones have been described as natural laboratories, because they allow us to understand how reproductive isolation and barriers to gene flow play out in the real world (Harrison, 1990). In addition, their presence provides compelling evidence for ongoing gene flow between the taxa being studied, the relative duration of which can now be estimated using demographic inference methods. Moreover, cline theory provides a rich, spatially explicit framework for studying selection and gene flow across porous species boundaries (Barton & Gale, 1993; Barton & Hewitt, 1985; Szymura & Barton, 1986). Specifically, the shape and position of geographic clines are impacted by the relative effects of selection and gene flow across a hybrid zone (Barton & Hewitt, 1985). Cline analysis has clear advantages over population genetic summary statistics used in most selection scans (e.g., F_{ST}), but it is only beginning to be applied to genome-scale data sets (Rafati et al., 2018; Singhal & Bi, 2017; Stankowski et al., 2017; Westram et al., 2018; Westram et al., 2021). In this study, we combine top-down and bottom-up analyses to investigate the phenotypic and genetic architecture of pollinator isolation between hybridizing ecotypes of the bush monkeyflower (*Mimulus aurantiacus*).

In San Diego County, California, USA, there is a sharp geographical transition between red- and yellow-flowered ecotypes of *M. aurantiacus* subsp. *puniceus* (Streisfeld & Kohn, 2005). Despite being very closely related (d_a = 0.005; Stankowski et al., 2019), the ecotypes show extensive divergence across a suite of floral traits, including colour, size, shape and placement of reproductive parts (Figure 1; Streisfeld & Kohn, 2005; Tulig, 2000; Waayers, 1996). Previous work suggests an important role for pollinators in driving floral trait divergence and reproductive isolation in this system (; Sobel & Streisfeld, 2015; Streisfeld et al., 2013; Streisfeld & Kohn, 2005, 2007). Field experiments have shown that hummingbirds and hawkmoths show strong preferences and constancy for the flowers of the red and yellow ecotypes, respectively (Sobel & Streisfeld, 2015; Streisfeld & Kohn, 2007). In addition to providing a source of divergent selection, pollinator behaviour generates substantial premating isolation, potentially reducing gene flow between the ecotypes by 78% in sympatry (Sobel & Streisfeld, 2015). Estimates of intrinsic postmating isolation in F_1 hybrids are weak, further suggesting that pollinator isolation is a primary barrier to gene flow in this system (Sobel & Streisfeld, 2015).

Although the strength of pollinator-mediated reproductive isolation is strong, it is incomplete, meaning that there is potential for gene flow between the ecotypes in locations where their distributions overlap. This has led to the formation of a narrow hybrid zone, characterized by extensive phenotypic variation and geographic clines in several floral traits. For example, there is a steep cline in flower colour that is centred on the hybrid zone and matches a similarly steep cline in the gene *MaMyb2*, which controls much of the variation in floral pigmentation (Streisfeld et al., 2013). Other floral traits and anonymous single-nucleotide polymorphisms (SNPs) also show clinal variation, implying that multiple traits contribute to reproductive isolation (Stankowski et al., 2015, 2017). However, the genomic positions of these SNPs and the genetic architecture of the trait variation were not established, making it impossible to test for an association between these phenotypic traits and genotypic signatures of selection.

In this study, we take advantage of recent genomic developments in this system (Stankowski et al., 2019) and use demographic modelling, a cline-based genome scan and QTL mapping to investigate the history of divergence and the phenotypic and genetic architectures of pollinator isolation in this system. One hypothesis

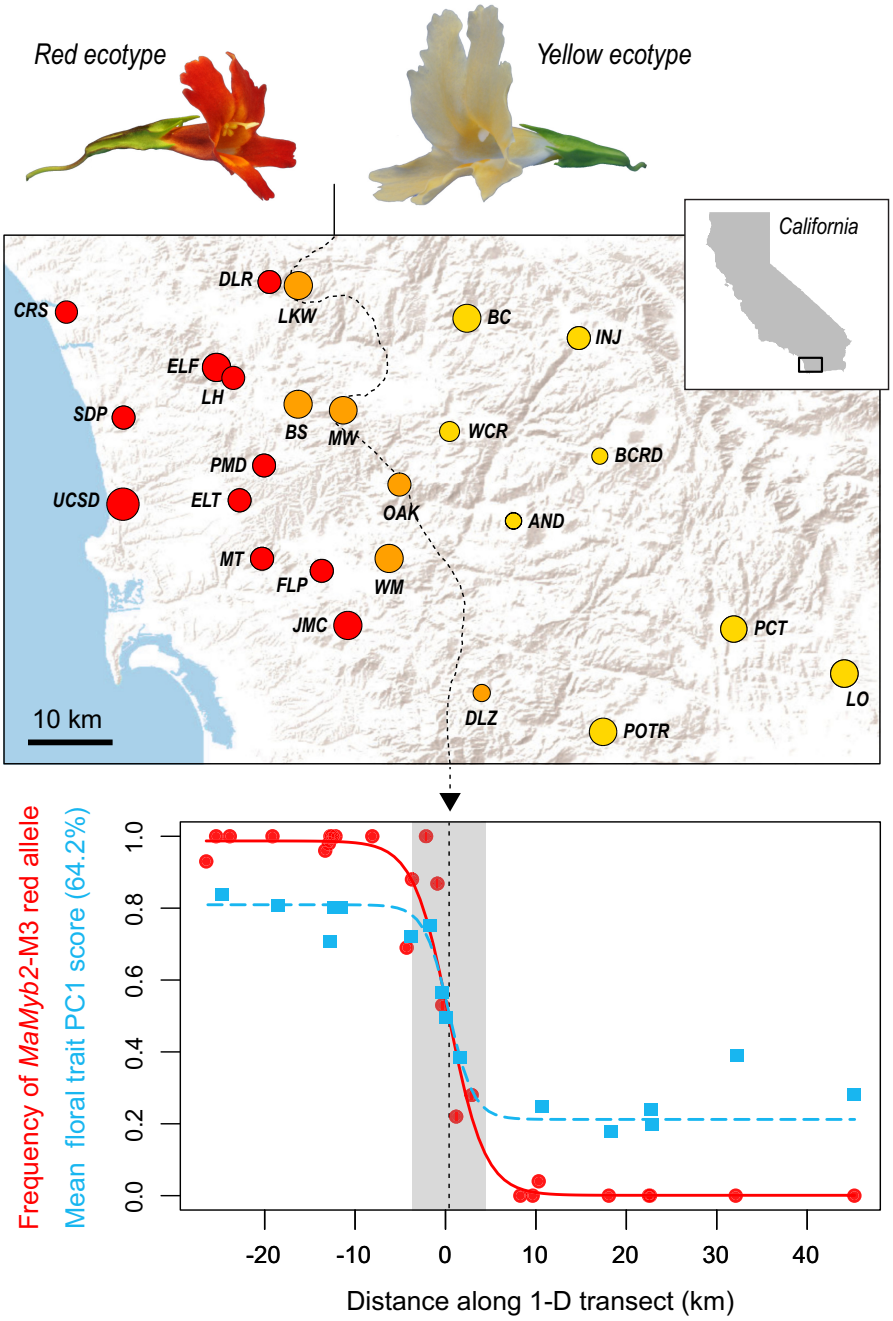

FIGURE 1 Clinal variation across a bush monkeyflower hybrid zone. (top) Typical flower phenotypes of the red and yellow ecotypes, and a map of the 25 sampling locations in San Diego County. The size of the circles shows variation in the sample sizes, which range from four to 18 individuals, totalling 294 individuals. The dashed line indicates the centre of the hybrid zone, previously inferred from spatial variation in the frequency of alternative alleles at the *MaMyb2* locus. (bottom) Clines in allele frequency at the *MaMyb2* locus (red circles) and the mean floral trait score for the first principal component (PC1; blue squares, computed from Stankowski et al., 2015) across the one-dimensional transect. The solid and dashed lines are the maximum-likelihood sigmoid cline models for *MaMyb2* allele frequency and trait PC1 score, respectively. The grey shaded rectangle represents the width of the hybrid zone. Figure re-created from Stankowski et al. (2017) with slight modifications.

is that QTL for the divergent phenotypes will overlap with regions of the genome under selection, as predicted if pollinator-mediated selection is the main barrier to gene flow between the ecotypes. These regions may be abundant and widespread across the genome, reflecting polygenic divergence, or they may consist of one or a few genomic regions enriched for loci that underlie multiple floral traits. Under an alternative scenario, we may find that floral QTL rarely overlap with genomic signatures of selection, which might reflect the spatial coupling of multiple different kinds of barriers. Our findings highlight the challenges of understanding the genetic architecture of reproductive isolation and suggest that barriers to gene flow other than pollinator isolation may also contribute to speciation in this system.

2 | METHODS

2.1 | RAD sequencing, read filtering, and SNP calling

We identified SNPs using previously sequenced restriction-site-associated DNA sequences (RADseq) from 294 individuals sampled from 25 locations across the hybrid zone (mean individuals per site = 12; range 4–18) (Stankowski et al., 2017). These included 11 sites in the range of the red ecotype, eight sites in the range of the yellow ecotype and six sites in the hybrid zone (Table S1).

We reprocessed the raw sequences to identify SNPs and call genotypes using STACKS version 1.41 (Catchen et al., 2013). Reads

were filtered based on quality, and errors in the barcode sequence or RAD site were corrected using the *process_radtags* script in STACKS. Individual reads were aligned to the *Mimulus aurantiacus* genome (Stankowski et al., 2019) using BOWTIE 2 (Langmead & Salzberg, 2012), with the *very_sensitive* settings. We identified SNPs using the *ref_map.pl* function of STACKS, with two identical reads required to create a stack and two mismatches allowed when processing the catalogue. SNP identification and genotype calls were conducted using the maximum-likelihood model (alpha = 0.01) (Hohenlohe et al., 2010). To include an SNP in the final data set, we required it to be present in at least 70% of all individuals; this resulted in a final data set of 219,152 SNPs.

2.2 | Demographic inference

To gain a deeper understanding of the history of gene flow and isolation in this system, we performed demographic inference in ∂A∂I (Gutenkunst et al., 2009). We calculated the unfolded joint site frequency spectrum (JSFS) based on 19,902 SNPs, using subspecies *grandiflorus* as an outgroup to polarize alleles as ancestral or derived (Chase et al., 2017). SNPs were included if they were genotyped in *grandiflorus* and in at least 70% of the red and yellow individuals. In addition, to reduce linkage disequilibrium (LD) among sites, markers were further thinned to a single SNP per RAD locus. We included 124 individuals from 10 sites of the red-flowered ecotype and 65 individuals from seven sites of the yellow-flowered ecotype, excluding sample sites that showed evidence of recent admixture (all hybrid sample sites and populations DLR and BC). The JSFS was projected to a sample size of 85 to maximize the number of segregating sites, as recommended in the manual.

We fit nine two-population demographic models to the JSFS (Figure S1) using analysis scripts published by Rougemont et al. (2017): (i) strict isolation (SI), (ii) ancient migration (AM), (iii) isolation with migration (IM), (iv) secondary contact (SC) and (v) periods of secondary contact (PSC). The remaining four models—(vi) AM2*m*, (vii) IM2*m*, (viii) SC2*m* and (ix) PSC2*m*—are the same as models ii–v, except that migration rates are inferred for two groups of loci to simulate the effect of a porous barrier to gene flow. Specifically, migration rate parameters were estimated by the model separately for two classes of loci: neutral loci and those that were associated with barriers to gene flow. If *2m* models fit the data better than the base models, this would support a conclusion of a heterogeneous barrier to gene flow, where a proportion of loci across the genome are capable of flowing between the ecotypes, but specific barrier loci impede gene flow elsewhere. For each model, we performed 20 independent runs using randomly generated starting parameters, with the search space constrained as in Rougemont et al. (2017). We report the results for the run with the lowest log-likelihood. The goodness of fit of the models was determined using the Akaike Information Criterion (AIC). Parameter estimates were converted into biologically meaningful values as described previously (Rougeux et al., 2017), assuming a mutation rate of 7×10^{-9} (Ossowski et al., 2010).

2.3 | Admixture analysis

We used the model-based clustering program ADMIXTURE (Alexander et al., 2009) to characterize patterns of genetic structure across the hybrid zone. We assigned the 294 individuals sampled from across San Diego County into two clusters ($K = 2$) based on the full data set of 219,152 SNPs (note that $K = 2$ was determined as the optimum number of clusters in Stankowski et al. (2017). In addition to using the full data set, we also pruned SNPs using the *--indep-pairwise* function in PLINK (Purcell et al., 2007) to reduce LD between neighbouring SNPs (r^2 threshold of 0.1, window size = 50 SNPs, step size = 10 SNPs).

We also ran ADMIXTURE separately for each chromosome, and for 2173 nonoverlapping windows, each containing 100 SNPs (mean window size of 89.1 kb, with 8–38 RAD tags per window; Figure S2). The window-based analysis was automated using custom python scripts to produce plink.map and .ped files for each consecutive window, which were then passed to ADMIXTURE.

2.4 | Cline fitting

Our previous work fit clines in allele frequency based on the most highly differentiated SNPs across the genome without reference to their genomic location (Stankowski et al., 2017). To take full advantage of this rich data set, which is now anchored to the reference genome, we quantified the geographical variation in ancestry (Q) by fitting a sigmoid cline model to the mean ancestry scores from each site. Sites were reduced to a one-dimensional west to east transect that was centred on the hybrid zone, as described in Stankowski et al. (2017) (Figure 1). Clines were fitted separately to the full data set, to each chromosome and to each 100-SNP window using the quantitative trait model in HZAR (Derryberry et al., 2014), with the variance in the trait modelled separately on the left side, centre and right side of the cline. We estimated the following parameters: the cline centre (*c*), defined as the inflection point of the sigmoid function; Q_{left} and Q_{right}, the mean ancestry scores on the left and right sides of the cline, respectively; and the cline width (*w*), defined as the ratio between the total change in ancestry across the cline (ΔQ) and the slope at the cline centre (note that $\Delta Q = Q_{left} - Q_{right}$ because we ensured that the mean ancestry score was higher on the left side before fitting). We conducted three independent fits with random starting values and retained the one with the highest log-likelihood. All of the best fits were visually inspected to ensure a sensible fit.

2.5 | Summarizing clinal variation in windows

After cline fitting, we calculated an ad hoc statistic to identify genomic windows that had clines with a similar shape and position to the genome-wide cline. We refer to this statistic as the cline similarity score (*cs* score). Unlike individual parameters (e.g., the width or centre), which describe a single feature of a cline, the

cs score describes the shape and relative position of a cline with a single number. We calculate the cline similarity score as: $cs = \left(\frac{\Delta Q}{w+l}\right) \times \left(e^{-(|c \div l|)}\right)^2$. Briefly (but see Appendix S1 for more details), the total change in ancestry, ΔQ, is divided by the sum of w and a scaling variable (l) to give an estimate of cline shape. The scaling variable controls the spread of shape scores across the joint distribution of ΔQ and w. In our case, l = half the length of the transect (0.5 t), which results in high shape scores when clines have high ΔQ and low w, but low shape scores when clines have low ΔQ and high w. The shape score is then scaled according to the position of the cline centre, c, relative to a position of interest. This could be a feature of the environment or a cline in a focal marker or trait. In our case, the position of interest is the centre of the genome-wide ancestry cline. If the cline centre coincides exactly with this point, then the shape score is equal to the *cs* score. However, the further that a cline centre is shifted away from the point of interest, the more the shape score is downgraded, resulting in a lower estimate of *cs*. Therefore, to have a high value of *cs*, a cline from a genomic window must have its shape and position closely match the cline in genome-wide ancestry (as in Figure 3a). Finally, we scaled the *cs* score relative to the genome-wide ancestry cline, where 1 is the *cs* score calculated for the genome-wide ancestry cline, and 0 is the minimum value of *cs* observed for a window.

2.6 | Estimates of genetic differentiation in genomic windows

To characterize levels of genetic differentiation in a more traditional way, we calculated the population genetic statistic F_{CT} between the ecotypes in each 100-SNP window using the program ARLEQUIN (Excoffier & Lischer, 2010). This was done in an analysis of molecular variance framework that partitioned genetic variation between the ecotypes, among populations within ecotypes, and within populations. Populations were classified as coming either from the red or yellow ecotypes based on the ADMIXTURE results. Samples from hybrid populations were excluded from this analysis. We compared the relationship between *cs* score and F_{CT} among windows using linear regression.

2.7 | QTL analysis

We used QTL analysis to identify genomic regions underlying divergent floral traits. We generated an outcrossed F_2 population that contained 292 offspring produced by crossing two F_1 individuals; each of these F_1 parents was produced by crossing different greenhouse-raised red and yellow ecotype plants (from populations UCSD and LO; Table S1). To allow direct phenotypic comparison among plants grown in a common environment, we raised 25 red ecotype individuals (location UCSD), 31 yellow ecotype individuals (location LO) and 20 F_1 individuals (LO × USCD) alongside the F_2 individuals. For each plant, we measured 13 floral traits (Figure S3). Plants were raised as described in Stankowski et al. (2015).

QTL mapping was conducted using R/QTL (Broman et al., 2003) and a previously published genetic map (Stankowski et al., 2019) generated from the same mapping population using LEP-MAP2 (Rastas et al., 2016). We used phase information from LEP-MAP2 to infer the grandparental origin of alleles in the F_2 individuals at 7574 mapped markers, which allowed us to recode them as coming either from a red or yellow grandparent. This set of markers was then reduced to 2631—one per map position—by retaining the marker at each map position with the least missing data. Missing data for these markers were inferred by imputation using phase information from the mapping software and confirmed manually in a subset of individuals. For each trait, we then used automated stepwise scanning for additive QTL and pairwise interactions using Haley–Knott regression and LOD penalties calculated for each trait using a permutation test as described in the manual. QTL identified using this procedure were then incorporated into a multi-QTL model to refine their positions, calculate 95% Bayes credible intervals and estimate the percentage phenotypic variation explained (i.e., the effect size) of each QTL.

2.8 | Test for an excess of QTL overlap

To test for co-localization among QTL, we used a permutation test to determine if there was significantly more overlap among QTL than expected by chance. We first estimated the observed number of overlaps based on the Bayes credible intervals among the 26 identified QTL using the *findOverlaps* function of the GENOMICRANGES package (Lawrence et al., 2013) in R and determined the average number of overlaps per QTL (*n* overlaps/*n* QTL). To determine if this statistic was significantly larger than expected by chance, we randomly generated new QTL positions while maintaining the observed number and size of observed QTL. We made the probability of QTL "landing" on a given chromosome (Chr) a function of that chromosome's length (L_i) relative to the total genome length (L_T), $P(\text{Chr}_i) = L_i/L_T$, so that larger chromosomes were more likely to have QTL i assigned to them. We calculated the mean number of overlaps per QTL for 9999 random data sets and estimated a p-value for the observed value as the number of permuted data sets where n overlaps/n QTL was equal to or greater than the observed estimate +1/number of permutations +1.

2.9 | Test for overlap of QTL and outlier windows

We also used a permutation test to determine if QTL regions were enriched for outliers identified in our cline- and F_{CT}-based genome scans. We first counted the observed number of outlier windows within the empirical QTL intervals. This was performed for both *cs* and F_{CT} outliers, defined using two different cutoffs (top 1% and 5% of the empirical distributions). To determine if these counts were significantly different from chance, we produced 9999 data sets where

the genomic position of outlier windows was randomized, and we counted the number of outliers falling inside the empirical QTL intervals. A *p*-value for the estimate was calculated as described above.

3 | RESULTS

3.1 | Evidence for secondary contact and heterogeneous gene flow

The results of our demographic modelling support a history of gene flow across the range of the ecotypes. First, demographic models that included contemporary gene flow were far better at recreating the observed JSFS than a model of divergence without gene flow (i.e., strict isolation; −ΔAIC = 3938), or the best model of ancient migration, which included historical but not contemporary gene flow (−ΔAIC = 1157) (Figure 2; Figure S4). Second, models that included heterogeneous migration across the genome (2*m*) were always strongly favoured over the equivalent models, where gene flow was modelled with a single rate (Figure 2). Third, the SC and PSC models, which included periods of allopatry and secondary contact, were strongly favoured over the IM model, where divergence occurred without a period of geographical isolation. The best-fitting model was the SC2*m* model, indicating that divergence of the red and yellow ecotypes included a period of allopatry followed by gene flow upon secondary contact (Figure 2). Assuming a mutation rate of 7×10^{-9} (Ossowski et al., 2010), the ML parameters indicate that the ecotypes have been exchanging an average of 37 migrants per generation (m_{YR} = 34.5 per generation; m_{RY} = 40.3 per generation) for the last 1800 generations, which equates to roughly 3600 years, based on a 2-year generation time for these perennial plants. Despite evidence that gene flow between the ecotypes has been extensive, the ML model suggests that 37.4% of loci have experienced a substantial reduction in effective migration (15–20-fold; m_{eYR} = 1.7 per generation; m_{eRY} = 2.7 per generation) due to the effects of selection against gene flow (Figure 2).

3.2 | Sharp clines in genome- and chromosome-wide ancestry

The presence of sharp clines in multiple floral traits suggests that some fraction of the genome is impacted by selection against gene flow (Stankowski et al., 2015). The results from ADMIXTURE support these findings, revealing genome-wide patterns of ancestry that closely match the ecotypic designations assigned based on floral phenotypes (Figure S5). Specifically, red- and yellow-flowered individuals sampled from either side of the hybrid zone were strongly assigned to alternate clusters, while individuals from hybrid populations tended to show some assignment to both clusters, indicating their genomes are a mix of red and yellow ancestry. The results are nearly identical between independent runs of ADMIXTURE that include the full data set or subsets of the data pruned to minimize LD between neighbouring SNPs ($r^2 > 0.999$).

To compare these changes in ancestry to the observed geographical variation in floral traits, we used cline analysis to fit a sigmoid cline to the mean ancestry scores from each site. The best-fitting cline model provides an excellent summary of the change in

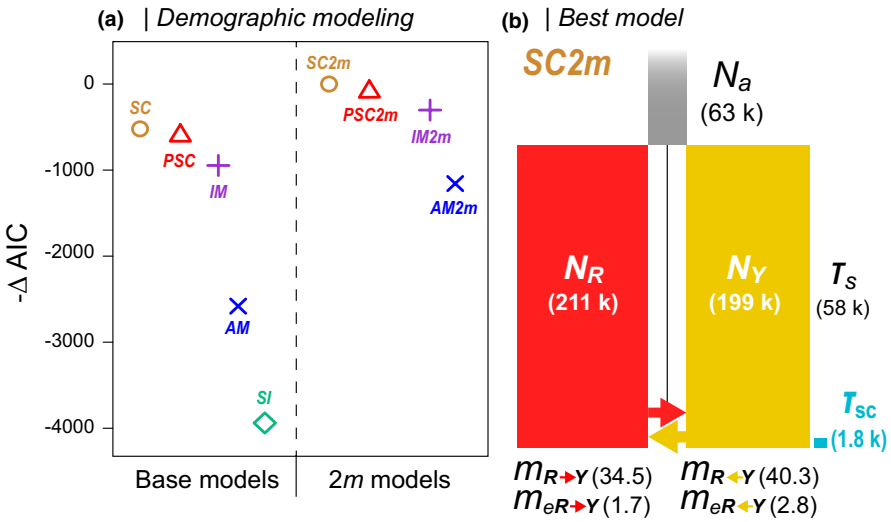

FIGURE 2 Demographic modelling reveals a history of gene flow following isolation. (a) -ΔAIC scores for the nine demographic models fitted to the observed JSFS using ∂A∂I. The base models (left of the dashed line) include a single migration parameter (*m*) for all loci, whereas the 2*m* models include separate migration parameters for neutral loci (*m*) and those affected by a barrier to gene flow (m_e, often referred to as effective migration). The best model (SC2*m*) has a -ΔAIC of 0, with more negative values indicating models with a poorer fit. (b) A graphical depiction of the SC2*m* model. The width of the columns is proportional to the population size estimates for the ancestral (N_a), red (N_R) and yellow (N_Y) populations. The height of the red and yellow bars is proportional to the total time in generations (T_S) that has passed since the split. The blue bar shows the period during which secondary gene flow (T_{SC}) occurred. The difference in arrow size is proportional to the difference in the bi-directional migration rate, *m*. The rates of effective migration (m_e) are too small to show graphically.

ancestry across the transect (Figure 3a) and has an extremely similar shape to cline models from the divergent floral traits and molecular markers (Figure 1). In addition, consistent with the increased variance we observed in multiple phenotypic traits in hybrid populations (Stankowski et al., 2015), the standard deviation of ancestry scores is higher in sample sites close to the cline centre, thus providing genomic evidence for hybridization (Figure 3a).

The ADMIXTURE scores provide additional genetic evidence for restricted gene flow across the hybrid zone, but they give us no indication as to the number of loci involved or their genomic distribution. For example, the differences in ancestry could be driven by a small number of loci that reside on a single chromosome, or they could reflect more widespread genomic divergence, involving loci scattered across multiple chromosomes. By repeating the cline analysis of ancestry scores separately for each chromosome, we find highly consistent clines in ancestry for all 10 chromosomes (Figure 3b; Figure S6).

3.3 | Heterogeneous clinal variation across the genome

To understand how cline shape varies at a finer genomic scale, we fit clines to 2173 nonoverlapping 100-SNP windows. This analysis revealed broad variation in geographical patterns of ancestry (Figure 3c). Unlike each chromosome, the majority of windows show little or no spatial change in ancestry between the red and yellow ecotypes, translating into very low *cs* scores (mean *cs* = 0.15; *SD* = 0.15, Figure 4).

Some genomic regions show clines in ancestry that strongly resemble the genome-wide cline, suggesting that they contain barrier loci. This includes the window with the highest *cs* score (*cs* = 0.91), which contains the known barrier locus, *MaMyb2*. The shape and position of this window-based ancestry cline (ΔQ = 0.95, *w* = 10.4 km, *c* = −0.3 km) is highly similar to the genome-wide cline in ancestry (ΔQ = 0.95, *w* = 7.6 km, *c* = 0.37 km) and to the cline in allele frequency for an SNP in *MaMyb2* (*MaMyb2*-M3 marker: Δ*P* = 0.99, *w* = 8.1 km, *c* = −0.07 km; Stankowski et al., 2017). However, rather than a clear set of outliers, we observe a continuous distribution of *cs* scores. Therefore, we use the top 1% and 5% of the distribution of *cs* scores to define sets of candidate windows potentially containing barrier loci.

Regardless of which cutoff we use, these candidate barrier regions are broadly distributed across the genome. For the 5% cutoff (109 windows), windows occurred on all 10 chromosomes (5–20 windows per chromosome; for the 1% cutoff [22 windows], they occurred on nine of the 10 chromosomes with one to four windows per chromosome). There were only 12 cases where candidate windows were directly adjacent, further indicating that they were broadly distributed along each chromosome. We also find that genetic differentiation is higher for candidate regions than for the genomic background (1% mean F_{CT} = 0.31, 5% mean F_{CT} = 0.23, overall mean F_{CT} = 0.07). However, F_{CT} explains only 38% of the variation in *cs* scores (Figure S7).

3.4 | Most candidate barrier traits are polygenic

We used QTL mapping to identify regions of the genome associated with candidate barrier traits. The 13 floral traits showed significant differences between pure red and yellow ecotype plants when grown in a common environment, with mean trait values differing by 0.9–7.1 standard deviations (Figure S8). A total of 26 QTL were identified. For nine traits, we identified more than one QTL (range two to four), and QTL were located on all 10 linkage groups, with LG 7 containing QTL for seven different traits (Figure 4; Table S2, Figure S9). On average, each QTL explained 9.9% of the variation in the F_2 population (range 1.82%–62.6%) (Figure S10), with an average total variation explained for each trait of 19.8%. The exception was a large-effect QTL for anthocyanin content on LG 4 that explained 62.6% of the variation and mapped to a region near the previously identified causal gene *MaMyb2* (Streisfeld et al., 2013). Thus, despite clear heritable differences in these traits, QTL analysis was able to explain only a modest amount of the segregating phenotypic variation, indicating that most traits have a polygenic architecture.

The presence of multiple QTL occurring on the same chromosome indicates that these regions may contribute to multiple traits, which would help maintain trait associations in hybrid offspring (Smadja & Butlin, 2011). Overall, we find that QTL do tend to colocalize more often than would be expected by chance (mean observed overlap of 3.23 QTL; mean permuted overlap = 2.51 QTL; *p* = .042; Figure S11). However, the effects of this colocalization are seen most strongly only for certain size-related traits (e.g., height of the tallest and shorter anthers) that remain highly correlated in the F_2 generation (*r* = .97) (Figure S12). By contrast, the average correlation coefficient among all other pairs of traits was much lower (mean absolute value of *r* = .25). Specifically, there are three overlapping QTL on LG 4 that control anthocyanin and carotenoid pigmentation, as well as corolla height, which span a total physical distance of only 76 kb. However, these traits show weak correlations in the F_2 population (anthocyanin vs. carotenoid: *r* = .18; anthocyanin vs. corolla height: *r* = −.20; carotenoid vs. corolla height: *r* = .19), indicating that the QTL overlap would have little effect on maintaining the phenotypic correlations where hybridization occurs.

3.5 | Low concordance between QTL and outlier regions

Finally, we tested for overlap between the floral trait QTL and the candidate barrier regions from the cline-based and F_{CT} genome scans. Using a permutation test, we tested whether genomic windows with higher *cs* scores tended to overlap with QTL more often than expected by chance. Regardless of which cutoff we used (e.g., top 1% or top 5% of *cs* scores), we found that floral trait QTL were not significantly enriched for candidate barrier regions (*p* > .3; Figure S13). This suggests a complex connection between

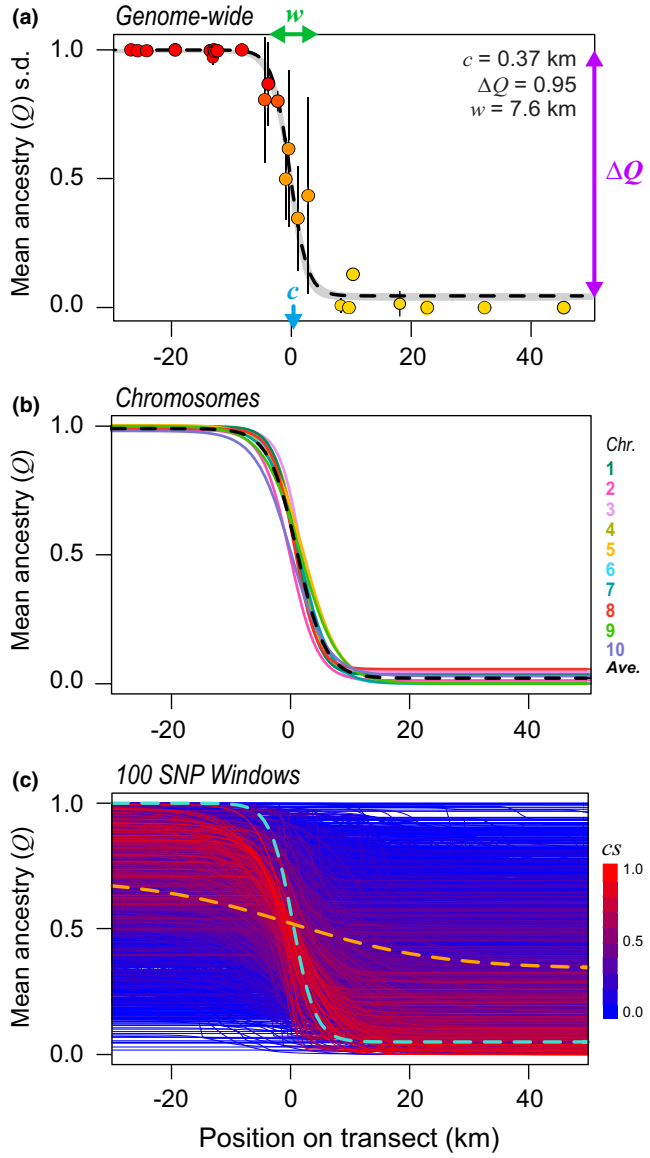

FIGURE 3 Clines in ancestry scores at different scales of genomic organization. (a) Genome-wide cline, inferred from the mean ancestry (Q) scores in each population along the 1-D transect. Position 0 on the horizontal axis corresponds to the cline centre estimated from *MaMyb2* allele frequencies (see Figure 1). The vertical bars show the standard deviation in ancestry scores for each population. The dashed line is the ML cline model, and the grey band is the two-unit support envelope. Three parameters of interest, including the cline centre (*c*), width (*w*) and total change in ancestry across the cline (ΔQ), are indicated on the plot. (b) Ancestry clines estimated separately for each chromosome. Only the ML curves are shown for clarity (but see Figure S6). The dashed line is the mean cline, estimated by taking the average of the ML parameters for all chromosomes. (c) Ancestry clines estimated for 2173, 100-SNP windows. The dashed cyan line shows the cline shape for the genome-wide cline (as shown in panel a), while the dashed orange line is the mean cline shape, estimated by taking the average of the ML parameters obtained for all windows. Each solid line is the ML sigmoid curve for one of the genomic windows. The curves are coloured according to the value of the cline similarity score (*cs*), which indicates how similar the shape and position of each cline are to the genome-wide cline. Redder clines are more similar to the genome-wide cline and bluer clines are less similar (see main text for more details).

the genetic and phenotypic architecture of reproductive isolation. The results were the same when we defined candidate barrier regions based on F_{CT} (e.g., top 1% or top 5% of the F_{CT} distribution; Figure S13).

Given that wide QTL intervals reduce the power of the enrichment test, we also asked how often the estimate of the QTL peak fell within a candidate barrier window. However, even when using the 5% cutoff, we found that none of the QTL peaks occurred within candidate barrier regions. This included the QTL for floral anthocyanin, where the QTL peak occurs 589 kb from the window containing the causal locus, *MaMyb2*.

4 | DISCUSSION

In this study, we used a combination of demographic modelling, QTL mapping and population genomic analyses to obtain a deeper understanding of the phenotypic and genetic architectures of reproductive isolation in a hybrid zone. Past studies in this system identified a large-effect locus responsible for flower colour differences that was under divergent selection across the hybrid zone (Stankowski & Streisfeld, 2015; Streisfeld et al., 2013). Additional candidate floral traits contributing to pollinator-mediated reproductive isolation also have been identified (Stankowski et al., 2015; Streisfeld & Kohn, 2007), but no candidate genes are known to be associated with these traits. Similarly, anonymous SNPs under selection have been discovered, but their genomic organization and association with candidate barrier traits were not established (Stankowski et al., 2017). Here, we use top-down and bottom-up approaches in an effort to connect genotype to phenotype and fitness. Our findings are discussed in light of the new insights obtained here regarding the history of divergence and are aided by the known, large-effect barrier locus (*MaMyb2*) that has a clear phenotypic effect.

4.1 | The history of divergence: New insights from demographic analysis

A firm understanding of the historical demography of speciation is essential when interpreting divergence across hybrid zones (Endler, 1977; Hewitt, 1988). In zones that are at demographic equilibrium, it is possible to interpret clines in terms of migration, selection, and drift and sampling effects (Barton & Hewitt, 1985). However, if hybrid zones formed recently, clines in neutral loci or traits can be steep initially, but they will decay over time (Barton & Hewitt, 1985). Previous work in this system revealed a pattern of isolation-by-distance across (and orthogonal to) the hybrid zone that was consistent with a long-term "stepping-stone" pattern of gene flow across the entire range of the study area (Stankowski et al., 2015). In fact, there was no evidence for substantial

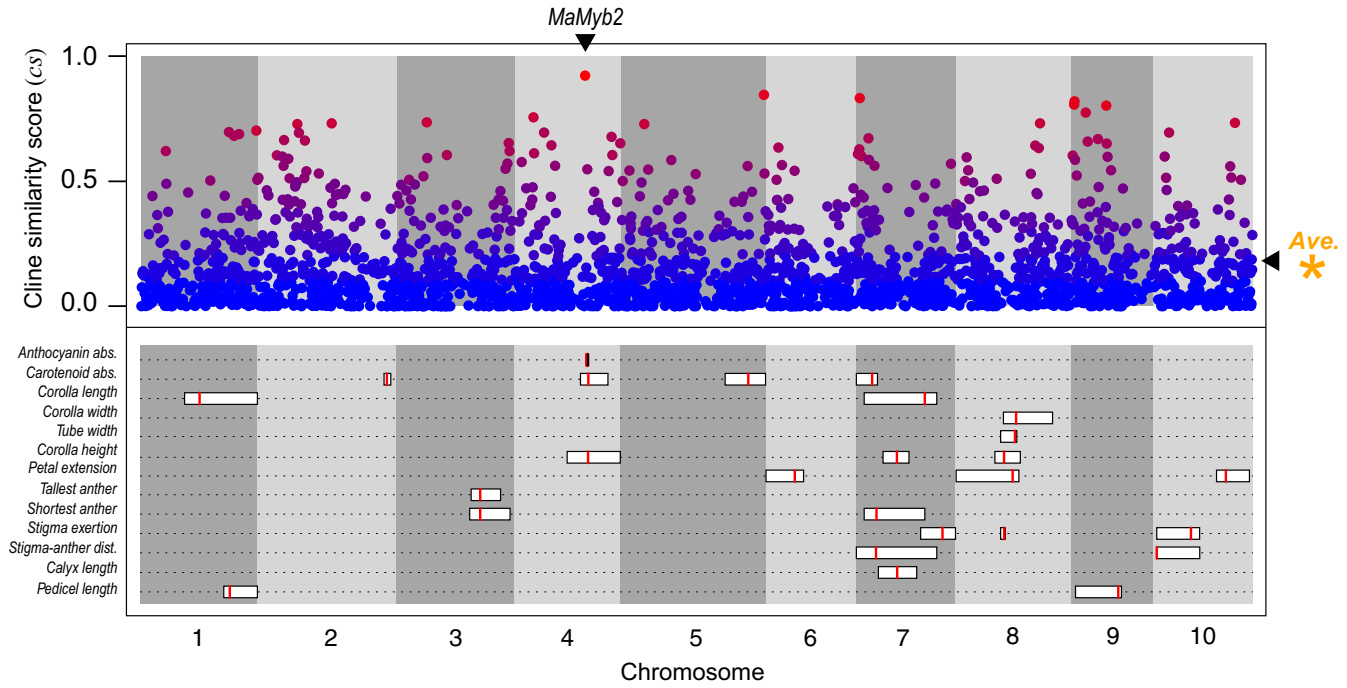

FIGURE 4 Cline-based genome scan and locations of QTL for floral traits. (top) The scaled cline similarity (*cs* score) score in each 100-SNP window plotted against the physical position of the window in the bush monkeyflower genome. The points are coloured as in Figure 3c, with redder points containing windows with *cs* scores that are more similar to the genome-wide pattern and bluer points are less similar (see main text for more details). The orange asterisk denotes the average cline similarity score among all windows. The position of the *MaMyb2* gene that controls differences in flower colour is shown. (bottom) The positions of the QTL for the 13 measured floral traits plotted along the physical position of the genome. The red vertical line corresponds to the best estimate of the QTL peak, and the width of the rectangles denotes the 95% Bayes credible intervals of the estimated QTL position.

genome-wide differentiation between the ecotypes after correcting for the effect of geography. Based on this result, Stankowski et al. (2015) concluded that the hybrid zone formed due to one of three possible scenarios: (i) a primary origin with continuous gene flow during divergence, (ii) a secondary origin, where divergence occurred in allopatry, followed by extensive gene flow after contact resumed, or (iii) a secondary origin where the period of allopatry was short.

Our demographic analyses provide new evidence that this hybrid zone formed from secondary contact after a relatively long period of isolation. Indeed, both models that included periods of geographical isolation (SC and PSC) were a better fit to the data than models of continuous gene flow (IM). The parameter estimates for the preferred model (SC2*m*) indicate a relatively long period of isolation, followed by a period of secondary contact that began roughly 1800 generations ago. It is important to note that we fit relatively simple models to the data that excluded changes in population size in the ancestral and daughter populations and variation in N_e along the genome. Recent work has shown that failure to model key parameters can result in incorrect inference under some circumstances (Momigliano et al., 2021). Although more sophisticated modelling may arrive at different conclusions in the future, these results clearly point to a secondary origin of this hybrid zone.

In terms of the main goal of our paper, another key result of the demographic analysis was that all models with two rates of migration (2*m* models) fit the data better than those where migration was modelled at a single rate. These findings indicate a heterogeneous pattern of gene flow across the genome, where some loci are able to flow freely between the ecotypes but others are impeded. Moreover, the estimated parameters for the preferred model suggest that more than one-third of loci (37%) have experienced migration at substantially reduced rate compared with non-barrier loci. This result supports previous conclusions that candidate barrier traits and loci are indeed impacted by natural selection (Stankowski et al., 2017), further motivating the need to understand the genetic architecture of reproductive isolation in more detail.

4.2 | From the "bottom up": Insights from the cline-based genome scan

We used a cline-based genome scan to identify 100-SNP windows across the genome that represent potential candidate loci corresponding to barriers to gene flow. Unlike traditional summary statistics (e.g., F_{ST}) or local ancestry approaches that are calculated between predefined groups of populations, geographic cline analysis only uses spatial information of populations along a transect to provide insight into the nature of selection across hybrid zones (Stankowski et al., 2017; Westram et al., 2018). However, rather than fitting clines to allele frequencies for individual SNPs, we fit clines to model-based ancestry scores, treating them as quantitative traits (Barton & Gale, 1993).

By conducting this analysis at different scales of genomic organization, we are able to conclude that candidate barrier regions are widespread throughout the genome. At the genome-wide scale, the cline in ancestry is centred on the hybrid zone and has a very similar shape to the clines in floral traits (Stankowski et al., 2015). At the chromosome scale, all 10 chromosomes show clear sigmoid clines in ancestry, with their shapes and positions also highly similar to the genome-wide cline. The window-based analysis also reveals individual regions present on all 10 chromosomes that have highly similar cline shapes and positions to the genome-wide cline in ancestry, revealing candidate barrier loci. The window with the highest *cs* score is located on chromosome 4 and contains the gene *MaMyb2*. Alternative alleles at this locus control the major difference in flower colour, and other population genetic analyses indicate that it has been subject to strong divergent selection (Stankowski & Streisfeld, 2015; Streisfeld et al., 2013). Prior knowledge of this barrier locus provides confidence that other windows with high *cs* scores also probably harbour barrier loci with similarly large phenotypic effects.

However, rather than identifying a clear set of *cs* outliers, we observed a continuous distribution of *cs* scores, indicating that clines show varying degrees of resemblance to the genome-wide cline. Although it is tempting to interpret variation in the cline similarity score exclusively in terms of the sieving effect of a porous species boundary (i.e., assuming that the *cs* score is proportional to a local reduction in gene flow caused by associated barrier loci), the observed variation in *cs* scores requires more conservative interpretation. First, neutral processes, such as isolation-by-distance, can generate clines that are similar to clines generated by selection (Westram et al., 2018). Similarly, neutral clines generated by secondary contact can take a long time to decay, making them hard to distinguish from selected ones (Barton & Hewitt, 1985; Endler, 1977). Localized drift (and sampling effects) tends to distort cline shapes in a way that may lead to the discovery of false positives (Jofre & Rosenthal, 2021; Polechova & Barton, 2011). In addition, even though a genomic region may contain a large-effect barrier locus, it might not show a cline if the genomic window is too broad to capture the relevant signatures. Future efforts to help identify non-neutral clines may be accomplished using whole-genome rather than reduced-representation sequencing, and by comparing results obtained from multiple hybrid zones (Westram et al., 2021). Simulations of cline formation could also help distinguish candidate outliers (as in Westram et al., 2018). Even with these measures in place, the noise generated by background processes and sampling effects may mean that we only have power to confidently detect large-effect loci, which remains a general problem with all genome scan approaches (Ravinet et al., 2017).

4.3 | From the "top down": Insights from QTL analysis of candidate isolating traits

We generated the first ever QTL map in this system to identify genomic regions underlying floral trait divergence. Although we identified a small number of QTL for each trait (between one and four), the identified QTL explained only about 20% of the variation in each trait. Given that these traits are under strong genetic control (Figure S8), the "missing" variance implies that most of the floral traits are polygenic, caused by many loci with effect sizes below our limit of detection. However, some fraction of the unexplained variation also may be due to epistatic interactions among loci or epigenetic or environmental differences experienced by each plant in the greenhouse.

Although finding many small-effect loci may be expected in studies of phenotypic evolution (Rockman, 2012), many analyses of adaptation and speciation have found distributions of effect sizes skewed toward larger effects (Griswold, 2006; Lenormand, 2002). Moreover, the identified regions often control more than one trait, and in some cases, more than one type of isolating barrier (e.g., pre- and postmating barriers). For example, in another pair of *Mimulus* species, *M. cardinalis* and *M. lewisii*, large-effect QTL for multiple traits associated with pollinator isolation and hybrid sterility occur in a few genomic regions thought to harbour chromosomal inversions (Fishman et al., 2013; Schemske & Bradshaw, 1999). In sunflowers (*Helianthus*), multiple traits are associated with local adaptation to dune and nondune habitats and map to a small number of large, nonrecombining haplotypes containing structural variants (Todesco et al., 2020) (for other examples see Hager et al., 2021; Jones et al., 2012; Lowry & Willis, 2010).

Large, multiple-effect loci are an expected outcome of local adaptation and speciation (Smadja & Butlin, 2011; Yeaman & Whitlock, 2011), because more "concentrated" genetic architectures are favoured in scenarios where gene flow opposes adaptive divergence (Yeaman & Whitlock, 2011). Not only do large-effect loci make individual traits more visible to selection, but tight linkage and pleiotropy enhance the coupling of different sets of adaptive traits, meaning that they can remain associated despite gene flow (Smadja & Butlin, 2011). This begs the question: why do we see so few large-effect loci and such little overlap among floral trait QTL in the red and yellow ecotypes? One potential explanation is that divergence was initiated during a period of geographical isolation—a hypothesis that is supported by our demographic analysis. If trait divergence did occur during a phase of allopatry, the selection favouring certain combinations of traits could build up LD among many small-effect loci without opposition by gene flow. Although the associations would decay rapidly upon secondary contact (as we see in the hybrid zone; Stankowski et al., 2015, 2017), this decay would be expected to occur over a spatial scale determined by the strength of selection and the migration rate. If two adjacent habitats occur over a scale that is many times larger than the dispersal distance of the organism (as is the case between the red and yellow ecotypes; Stankowski et al., 2015), then hybridization has almost no bearing on adaptation occurring in distant parts of the range (Barton, 2010). This makes divergence in parapatry almost as easy as in allopatry (Barton, 2013), meaning that local adaptation will persist far from the hybrid zone, and strong associations among small-effect loci can remain in all regions except for those closest to the hybrid zone.

Another factor that may have influenced the outcome of our QTL analysis is that the parents we used for mapping came from populations located very far from the hybrid zone. Because concentrated genetic architectures evolve as a response to gene flow (Yeaman & Whitlock, 2011), theory predicts that the genetic architecture of local adaptation may vary spatially in a way that reflects the local hybridization risk. This was highlighted in a hybrid zone between two ecologically differentiated subspecies of *Boechera stricta* (Lee et al., 2017). In the vicinity of the hybrid zone, several phenological traits map to a single locus containing a chromosomal inversion, where the ecotypes are differentially fixed for the standard and inverted arrangements. However, in areas that are more distant to the hybrid zone, both ecotypes harbour the standard arrangement, and QTL mapping with these populations revealed distinct QTL. Although it is possible that the genetic architecture of divergence also varies across the range of the red and yellow ecotypes in a way that might favour divergence, our observations suggest that this is unlikely. Specifically, there is no evidence for the phenotypic maintenance of two distinct ecotypic forms within the hybrid zone. Instead, we see a continuum of phenotypic variation that resembles what we observe in the F_2 mapping population (Stankowski et al., 2015), suggesting a similarly complex genetic architecture across the range.

4.4 | Inferences from integrating top-down and bottom-up approaches

Having identified a set of candidate barrier loci and QTL regions for putative barrier traits, we next sought to understand how they were connected in relation to previous hypotheses about reproductive isolation in this system (Stankowski et al., 2017). Taken at face value, the two analyses seem consistent, as they both suggest that divergence in this system is polygenic, involving regions spread across the genome. However, when we intersect the regions identified by these approaches, we find very little concordance. What does this tell us about divergence in this system?

First, there are some technical and biological explanations that could account for these findings. The first is that QTL analysis often has low resolution. Specifically, the QTL intervals are very wide, substantially reducing our power to test if QTL regions are enriched for candidate barrier loci. We see the same result if we focus on the estimated location of the QTL peaks, which never fall inside a candidate barrier region. This is even true for the peak of the large-effect QTL for floral anthocyanin pigmentation, which is located 589 kb from the window with the highest *cs* score that contains the *MaMyb2* gene responsible for the major difference in flower colour (Streisfeld et al., 2013). Therefore, had we not had a priori knowledge about the position of the gene from previous work, it is likely we would have failed to connect this strong signal of selection with the underlying gene involved. In addition, our genome scan is based on RADseq data, so the SNP density may have been too sparse to obtain sequences in LD with other loci under selection. Moreover, from a biological perspective, the QTL analysis implies that most of the traits studied are polygenic, meaning that selection on each locus is weak, making it difficult to detect them using any genome scan (Ravinet et al., 2017). All of these factors probably contribute to the highly complex pattern that we see.

Similarly, although many of the candidate barrier loci have clines that resemble the window that contains the large-effect locus *MaMyb2*, these windows are not associated with identified QTL for floral traits. One possible explanation for this is that we may have failed to measure the relevant floral traits contributing to pollinator isolation. This seems unlikely, given how well floral morphology has been studied in this system (Stankowski et al., 2015; Streisfeld & Kohn, 2005; Tulig, 2000; Waayers, 1996). We therefore hypothesize that other barriers to gene flow, besides pollinator isolation, play an important role in the maintenance of this hybrid zone. For example, local adaptation of non-floral traits could be an important source of pre- and postmating isolation (Coyne & Orr, 2004; Sobel et al., 2010). We previously identified clines in several ecophysiological traits that may be associated with habitat-based isolation (Sobel et al., 2019), but these show very shallow linear gradients rather than sharp sigmoid clines, making them unlikely candidates (Sobel et al., 2019). However, other ecologically based barriers may exist that remain to be characterized. Finally, it is possible that some of the candidate barrier regions contain intrinsic incompatibilities that cause reduced fitness in hybrids (Kulmuni & Westram, 2017). Although our previous work found little evidence for intrinsic postzygotic isolation in the F_1 generation, we did detect partial male sterility in some interecotype crosses (Sobel & Streisfeld, 2015). In addition, we have only surveyed plants under benign greenhouse conditions and only through the F_1 generation. Genetic incompatibilities in later generations (Stelkens et al., 2015) or under natural conditions (Thompson et al., 2022) might play a larger role in the maintenance of the ecotypes than anticipated—a prediction that has been made in relation to "ecological speciation" more broadly (Bierne et al., 2011).

4.5 | Conclusions and implications for studying the architecture of speciation

By combining top-down and bottom-up approaches with demographic modelling, our study provides new insight into the history and genetic architecture of speciation between these monkeyflower ecotypes. Our demographic analysis suggests that the hybrid zone formed by secondary contact, but the effects of multiple barrier loci result in a heterogeneous pattern of gene flow across the genome. A cline-based genome scan indicates that candidate barrier loci are widespread across the genome, rather than being associated with one or a few "islands" of speciation. Consistent with this finding, a QTL analysis of floral traits identified many QTL of small effect, with limited colocalization among QTL for different traits. However, we found limited evidence that QTL and candidate barrier loci overlap, suggesting that other barriers to gene flow apart from pollinator isolation may contribute to speciation.

In addition to generating new knowledge about this system, our study has important implications for efforts to understand the phenotypic and genetic architecture of isolating barriers. For many study systems, candidate barrier traits and loci are identified in separate studies, meaning that the link between them is not tested explicitly. However, any barrier locus associated with an ecological gradient may underlie a completely different type of barrier. This was highlighted by Bierne et al. (2011), who showed how intrinsic barriers can become spatially coupled with ecologically based barriers—a phenomenon that may cause researchers to erroneously identify incompatibility loci as those underlying local adaptation. The same issue also arises if multiple ecological gradients change in concert. We therefore advocate for additional studies that integrate top-down and bottom-up approaches, but we caution that these scenarios must be considered carefully before drawing strong conclusions about causal associations between candidate barrier traits and loci. Finally, our study shows that, even with a concerted effort, understanding the phenotypic and genetic basis of speciation is extremely difficult. Although emerging methods and data may help, this will probably remain a major challenge for the field.

AUTHOR CONTRIBUTIONS

SS and MAS designed the study and conducted the molecular work. SS and HM performed the QTL analysis. SS, MAC and MAS conducted all other analyses. SS and MAS wrote the manuscript, with input from the other authors.

ACKNOWLEDGEMENTS

We thank Julian Catchen for making modifications to Stacks to aid this project. Peter L. Ralph, Thomas Nelson, Roger K. Butlin, Anja M. Westram and Nicholas H. Barton provided advice, stimulating discussion and critical feedback. The project was supported by National Science Foundation grant DEB-1258199.

CONFLICT OF INTEREST

The authors declare no competing financial interests.

DATA AVAILABILITY STATEMENT

Sequence data are available on the short read archive (SRA) under bio projects PRJNA299226 and PRJNA317601. All other datafiles are available on Dryad (doi:10.5061/dryad.931zcrjq0). Scripts for performing custom analyses are available at https://github.com/seanstankowski/Mimulus_clines2

ORCID

Madeline A. Chase https://orcid.org/0000-0002-7916-3560
Matthew A. Streisfeld https://orcid.org/0000-0002-2660-8642

REFERENCES

Abbott, R., Albach, D., Ansell, S., Arntzen, J. W., Baird, S. J. E., Bierne, N., … Zinner, D. (2013). Hybridization and speciation. *Journal of Evolutionary Biology*, *26*(2), 229–246. https://doi.org/10.1111/j.1420-9101.2012.02599.x

Alexander, D. H., Novembre, J., & Lange, K. (2009). Fast model-based estimation of ancestry in unrelated individuals. *Genome Research*, *19*(9), 1655–1664. https://doi.org/10.1101/gr.094052.109

Barrett, R. D. H., & Hoekstra, H. E. (2012). Molecular spandrels: Tests of adaptation at the genetic level (vol 12, pg 767, 2011). *Nature Reviews Genetics*, *13*(1), 70–70. https://doi.org/10.1038/nrg3138

Barton, N. H. (2010). What role does natural selection play in speciation? *Philosophical Transactions of the Royal Society, B: Biological Sciences*, *365*(1547), 1825–1840. https://doi.org/10.1098/rstb.2010.0001

Barton, N. H. (2013). Does hybridization influence speciation? *Journal of Evolutionary Biology*, *26*(2), 267–269. https://doi.org/10.1111/jeb.12015

Barton, N. H., & Gale, K. S. (1993). Genetic analysis of hybrd zones. In *Hybrid zones and evolutionary process* (pp. 13–45). Oxford University Press.

Barton, N. H., & Hewitt, G. M. (1985). Analysis of hybrid zones. *Annual Review of Ecology and Systematics*, *16*, 113–148. https://doi.org/10.1146/annurev.es.16.110185.000553

Bierne, N., Welch, J., Loire, E., Bonhomme, F., & David, P. (2011). The coupling hypothesis: Why genome scans may fail to map local adaptation genes. *Molecular Ecology*, *20*(10), 2044–2072. https://doi.org/10.1111/j.1365-294X.2011.05080.x

Broman, K. W., Wu, H., Sen, S., & Churchill, G. A. (2003). R/qtl: QTL mapping in experimental crosses. *Bioinformatics*, *19*(7), 889–890. https://doi.org/10.1093/bioinformatics/btg112

Butlin, R. K., & Smadja, C. M. (2018). Coupling, reinforcement, and speciation. *American Naturalist*, *191*(2), 155–172. https://doi.org/10.1086/695136

Catchen, J., Hohenlohe, P. A., Bassham, S., Amores, A., & Cresko, W. A. (2013). Stacks: An analysis tool set for population genomics. [research support, N.I.H., extramural research support, U.S. Gov't, non-P.H.S. research support, U.S. Gov't, P.H.S.]. *Molecular Ecology*, *22*(11), 3124–3140. https://doi.org/10.1111/mec.12354

Chase, M. A., Stankowski, S., & Streisfeld, M. A. (2017). Genomewide variation provides insight into evolutionary relationships in a monkeyflower species complex (Mimulus sect. Diplacus). *American Journal of Botany*, *104*(10), 1510–1521. https://doi.org/10.3732/ajb.1700234

Coyne, J. A., & Orr, H. A. (2004). *Speciation*. Sinauer Associates.

Cruickshank, T. E., & Hahn, M. W. (2014). Reanalysis suggests that genomic islands of speciation are due to reduced diversity, not reduced gene flow. [research support, U.S. Gov't, non-P.H.S. review]. *Molecular Ecology*, *23*(13), 3133–3157. https://doi.org/10.1111/mec.12796

Derryberry, E. P., Derryberry, G. E., Maley, J. M., & Brumfield, R. T. (2014). Hzar: Hybrid zone analysis using an R software package. *Molecular Ecology Resources*, *14*(3), 652–663. https://doi.org/10.1111/1755-0998.12209

Endler, J. A. (1977). *Geographic variation, speciation, and clines*. Princeton University Press.

Excoffier, L., & Lischer, H. E. L. (2010). Arlequin suite ver 3.5: A new series of programs to perform population genetics analyses under Linux and windows. *Molecular Ecology Resources*, *10*(3), 564–567. https://doi.org/10.1111/j.1755-0998.2010.02847.x

Faria, R., Johannesson, K., & Stankowski, S. (2021). Speciation in marine environments: Diving under the surface. *Journal of Evolutionary Biology*, *34*(1), 4–15. https://doi.org/10.1111/jeb.13756

Fishman, L., Stathos, A., Beardsley, P. M., Williams, C. F., & Hill, J. P. (2013). Chromosomal rearrangements and the genetics of reproductive barriers in Mimulus (monkey flowers). *Evolution*, *67*(9), 2547–2560. https://doi.org/10.1111/evo.12154

Fishman, L., & Willis, J. H. (2001). Evidence for Dobzhansky-Muller incompatibilites contributing to the sterility of hybrids between *Mimulus guttatus* and M-nasutus. *Evolution*, *55*(10), 1932–1942.

Griswold, C. K. (2006). Gene flow's effect on the genetic architecture of a local adaptation and its consequences for QTL analyses. *Heredity*, *96*(6), 445–453. https://doi.org/10.1038/sj.hdy.6800822

Gutenkunst, R. N., Hernandez, R. D., Williamson, S. H., & Bustamante, C. D. (2009). Inferring the joint demographic history of multiple populations from multidimensional SNP frequency data. *PLoS Genetics*, *5*(10), e1000695. doi:10.1371/journal.pgen.1000695

Hager, E. R., Harringmeyer, O. S., Wooldridge, T. B., Theingi, S., Gable, J. T., McFadden, S., … Hoekstra, H. E. (2021). A chromosomal inversion drives evolution of multiple adaptive traits in deer mice. *bioRxiv*. https://doi.org/10.1101/2021.01.21.427490

Harrison, R. G. (1990). Hybrid zones: Windows on evolutionary process. *Oxford Surveys in Evolutionary Biology*, *7*, 69–128.

Hewitt, G. M. (1988). Hybrid zones—natural laboratories for evolutionary studies. *Trends in Ecology and Evolution*, *3*(7), 158–167. https://doi.org/10.1016/0169-5347(88)90033-X

Hohenlohe, P. A., Bassham, S., Etter, P. D., Stiffler, N., Johnson, E. A., & Cresko, W. A. (2010). Population genomics of parallel adaptation in Threespine stickleback using sequenced RAD tags. *PLoS Genetics*, *6*(2), e1000862. https://doi.org/10.1371/journal.pgen.1000862

Jofre, G. I., & Rosenthal, G. G. (2021). A narrow window for geographical cline analysis using genomic data: Effects of age, drift, and migration on error rates. *Molecular Ecology Resources*, *21*(7), 2278–2287. https://doi.org/10.1111/1755-0998.13428

Jones, F. C., Grabherr, M. G., Chan, Y. F., Russell, P., Mauceli, E., Johnson, J., Swofford, R., Pirun, M., Zody, M. C., White, S., & Birney, E. (2012). The genomic basis of adaptive evolution in threespine sticklebacks. *Nature*, *484*(7392), 55–61. https://doi.org/10.1038/nature10944

Kulmuni, J., & Westram, A. M. (2017). Intrinsic incompatibilities evolving as a by-product of divergent ecological selection: Considering them in empirical studies on divergence with gene flow. *Molecular Ecology*, *26*(12), 3093–3103. https://doi.org/10.1111/mec.14147

Lamichhaney, S., Berglund, J., Almen, M. S., Maqbool, K., Grabherr, M., Martinez-Barrio, A., … Andersson, L. (2015). Evolution of Darwin's finches and their beaks revealed by genome sequencing. [research support, non-U.S. Gov't]. *Nature*, *518*(7539), 371–375. https://doi.org/10.1038/nature14181

Langmead, B., & Salzberg, S. L. (2012). Fast gapped-read alignment with bowtie 2. *Nature Methods*, *9*(4), 357–359. https://doi.org/10.1038/Nmeth.1923

Lawrence, M., Huber, W., Pagès, H., Aboyoun, P., Carlson, M., Gentleman, R., Morgan, M. T., & Carey, V. J. (2013). Software for computing and annotating genomic ranges. *PLoS Computational Biology*, *9*(8), e1003118. https://doi.org/10.1371/journal.pcbi.1003118

Lee, C. R., Wang, B. S., Mojica, J. P., Mandáková, T., Prasad, K. Y. S. K., Goicoechea, J. L., Perera, N., Hellsten, U., Hundley, H. N., Johnson, J., Grimwood, J., Barry, K., Fairclough, S., Jenkins, J. W., Yu, Y., Kudrna, D., Zhang, J., Talag, J., Golser, W., … Mitchell-Olds, T. (2017). Young inversion with multiple linked QTLs under selection in a hybrid zone. *Nature Ecology and Evolution*, *1*(5), 1–13. https://doi.org/10.1038/S41559-017-0119

Lenormand, T. (2002). Gene flow and the limits to natural selection. *Trends in Ecology and Evolution*, *17*(4), 183–189. https://doi.org/10.1016/S0169-5347(02)02497-7

Lowry, D. B., & Willis, J. H. (2010). A widespread chromosomal inversion polymorphism contributes to a major life-history transition, local adaptation, and reproductive isolation. *PLoS Biology*, *8*(9), e1000500. https://doi.org/10.1371/journal.pbio.1000500

Martin, S. H., Dasmahapatra, K. K., Nadeau, N. J., Salazar, C., Walters, J. R., Simpson, F., Blaxter, M., Manica, A., Mallet, J., & Jiggins, C. D. (2013). Genome-wide evidence for speciation with gene flow in Heliconius butterflies. *Genome Research*, *23*(11), 1817–1828. https://doi.org/10.1101/gr.159426.113

Momigliano, P., Florin, A. B., & Merila, J. (2021). Biases in demographic modeling affect our understanding of recent divergence. *Molecular Biology and Evolution*, *38*(7), 2967–2985. https://doi.org/10.1093/molbev/msab047

Noor, M. A. F., & Bennett, S. M. (2009). Islands of speciation or mirages in the desert? Examining the role of restricted recombination in maintaining species. *Heredity*, *103*, 439–444. https://doi.org/10.1038/hdy.2009.151

Nosil, P. (2012). *Ecological Speciation*. Oxford University Press.

Orr, H. A. (2001). The genetics of species differences. *Trends in Ecology and Evolution*, *16*(7), 343–350.

Ossowski, S., Schneeberger, K., Lucas-Lledó, J. I., Warthmann, N., Clark, R. M., Shaw, R. G., Weigel, D., & Lynch, M. (2010). The rate and molecular Spectrum of spontaneous mutations in Arabidopsis thaliana. *Science*, *327*(5961), 92–94. https://doi.org/10.1126/science.1180677

Polechova, J., & Barton, N. (2011). Genetic drift widens the expected cline but narrows the expected cline width. *Genetics*, *189*(1), 227–235. https://doi.org/10.1534/genetics.111.129817

Purcell, S., Neale, B., Todd-Brown, K., Thomas, L., Ferreira, M. A. R., Bender, D., Maller, J., Sklar, P., de Bakker, P. I., Daly, M. J., & Sham, P. C. (2007). PLINK: A tool set for whole-genome association and population-based linkage analyses. *American Journal of Human Genetics*, *81*(3), 559–575. https://doi.org/10.1086/519795

Rafati, N., Blanco-Aguiar, J. A., Rubin, C. J., Sayyab, S., Sabatino, S. J., Afonso, S., Feng, C., Alves, P. C., Villafuerte, R., Ferrand, N., Andersson, L., & Carneiro, M. (2018). A genomic map of clinal variation across the European rabbit hybrid zone. *Molecular Ecology*, *27*(6), 1457–1478. https://doi.org/10.1111/mec.14494

Rastas, P., Calboli, F. C. F., Guo, B. C., Shikano, T., & Merila, J. (2016). Construction of Ultradense linkage maps with Lep-MAP2: Stickleback F-2 recombinant crosses as an example. *Genome Biology and Evolution*, *8*(1), 78–93. https://doi.org/10.1093/gbe/evv250

Ravinet, M., Faria, R., Butlin, R. K., Galindo, J., Bierne, N., Rafajlović, M., Noor, M. A. F., Mehlig, B., & Westram, A. M. (2017). Interpreting the genomic landscape of speciation: A road map for finding barriers to gene flow. *Journal of Evolutionary Biology*, *30*(8), 1450–1477. https://doi.org/10.1111/jeb.13047

Rockman, M. V. (2012). The Qtn program and the alleles that matter for evolution: All that's gold does not glitter. *Evolution*, *66*(1), 1–17. https://doi.org/10.1111/j.1558-5646.2011.01486.x

Rougemont, Q., Gagnaire, P., Perrier, P., Genthon, C., Besnard, A., Launey, S., & Evanno, G. (2017). Inferring the demographic history underlying parallel genomic divergence among pairs of parasitic and nonparasitic lamprey ecotypes. *Molecular Ecology*, *26*(1), 142–162. https://doi.org/10.1111/mec.13664

Rougeux, C., Bernatchez, L., & Gagnaire, P. A. (2017). Modeling the multiple facets of speciation-with-gene-flow toward inferring the divergence history of Lake whitefish species pairs (*Coregonus clupeaformis*). *Genome Biology and Evolution*, *9*(8), 2057–2074. https://doi.org/10.1093/gbe/evx150

Schemske, D. W., & Bradshaw, H. D. (1999). Pollinator preference and the evolution of floral traits in monkeyflowers (Mimulus). *Proceedings of the National Academy of Sciences of the United States of America*, *96*(21), 11910–11915. https://doi.org/10.1073/pnas.96.21.11910

Seehausen, O., Butlin, R. K., Keller, I., Wagner, C. E., Boughman, J. W., Hohenlohe, P. A., … Widmer, A. (2014). Genomics and the origin of species. *Nature Reviews Genetics*, *15*(3), 176–192. https://doi.org/10.1038/nrg3644

Singhal, S., & Bi, K. (2017). History cleans up messes: The impact of time in driving divergence and introgression in a tropical suture zone. *Evolution*, *71*(7), 1888–1899. https://doi.org/10.1111/evo.13278

Smadja, C. M., & Butlin, R. K. (2011). A framework for comparing processes of speciation in the presence of gene flow. *Molecular Ecology*, *20*(24), 5123–5140. https://doi.org/10.1111/j.1365-294X.2011.05350.x

Sobel, J. M., Chen, G. F., Watt, L. R., & Schemske, D. W. (2010). The biology of speciation. *Evolution*, *64*(2), 295–315. https://doi.org/10.1111/j.1558-5646.2009.00877.x

Sobel, J. M., Stankowski, S., & Streisfeld, M. A. (2019). Variation in ecophysiological traits might contribute to ecogeographic isolation and divergence between parapatric ecotypes of Mimulus aurantiacus. *Journal of Evolutionary Biology*, *32*(6), 604–618. https://doi.org/10.1111/jeb.13442

Sobel, J. M., & Streisfeld, M. A. (2015). Strong premating reproductive isolation drives incipient speciation in *Mimulus aurantiacus*. *Evolution*, *69*(2), 447–461. https://doi.org/10.1111/evo.12589

Soria-Carrasco, V., Gompert, Z., Comeault, A. A., Farkas, T. E., Parchman, T. L., Johnston, J. S., Buerkle, C. A., Feder, J. L., Bast, J., Schwander, T., Egan, S. P., Crespi, B. J., & Nosil, P. (2014). Stick insect genomes reveal natural Selection's role in parallel speciation. *Science*, *344*(6185), 738–742. https://doi.org/10.1126/science.1252136

Stankowski, S., Chase, M. A., Fuiten, A. M., Rodrigues, M. F., Ralph, P. L., & Streisfeld, M. A. (2019). Widespread selection and gene flow shape the genomic landscape during a radiation of monkeyflowers. *PLoS Biology*, *17*(7), e3000391. https://doi.org/10.1371/journal.pbio.3000391

Stankowski, S., & Ravinet, M. (2021). Defining the speciation continuum. *Evolution*, *75*(6), 1256–1273. https://doi.org/10.1111/evo.14215

Stankowski, S., Sobel, J. M., & Streisfeld, M. A. (2015). The geography of divergence with gene flow facilitates multitrait adaptation and the evolution of pollinator isolation in *Mimulus aurantiacus*. *Evolution*, *69*(12), 3054–3068. https://doi.org/10.1111/evo.12807

Stankowski, S., Sobel, J. M., & Streisfeld, M. A. (2017). Geographic cline analysis as a tool for studying genome-wide variation: A case study of pollinator-mediated divergence in a monkeyflower. *Molecular Ecology*, *26*(1), 107–122. https://doi.org/10.1111/mec.13645

Stankowski, S., & Streisfeld, M. A. (2015). Introgressive hybridization facilitates adaptive divergence in a recent radiation of monkeyflowers. *Proceedings of the Royal Society B: Biological Sciences*, *282*(1814), 154–162. https://doi.org/10.1098/Rspb.2015.1666

Stelkens, R. B., Schmid, C., & Seehausen, O. (2015). Hybrid breakdown in cichlid fish. *PLoS One*, *10*(5), e0127207. https://doi.org/10.1371/journal.pone.0127207

Streisfeld, M. A., & Kohn, J. R. (2005). Contrasting patterns of floral and molecular variation across a cline in Mimulus aurantiacus. *Evolution*, *59*(12), 2548–2559.

Streisfeld, M. A., & Kohn, J. R. (2007). Environment and pollinator-mediated selection on parapatric floral races of Mimulus aurantiacus. *Journal of Evolutionary Biology*, *20*(1), 122–132. https://doi.org/10.1111/j.1420-9101.2006.01216.x

Streisfeld, M. A., Young, W. N., & Sobel, J. M. (2013). Divergent selection drives genetic differentiation in an R2R3-MYB transcription factor that contributes to incipient speciation in Mimulus aurantiacus. *PLoS Genetics*, *9*(3), e1003385. https://doi.org/10.1371/journal.pgen.1003385

Szymura, J. M., & Barton, N. H. (1986). Genetic-analysis of a hybrid zone between the fire-bellied toads, Bombina-Bombina and Bombina-Variegata, near Cracow in southern Poland. *Evolution*, *40*(6), 1141–1159. https://doi.org/10.2307/2408943

Thompson, K., Peichel, C. H., Rennison, D. K., McGee, M. R., Albert, A. Y. K., Vines, T., Greenwood, A. K., Wark, A. R., Brandvain, Y., Schumer, M., & Schluter, D. (2022). Analysis of ancestry heterozygosity suggests that hybrid incompatibilities in threespine stickleback are environment dependent. *PLoS Biology*, *20*(1), e3001469. https://doi.org/10.1371/journal.pbio.3001469

Todesco, M., Owens, G. L., Bercovich, N., Légaré, J. S., Soudi, S., Burge, D. O., Huang, K., Ostevik, K. L., Drummond, E. B. M., Imerovski, I., Lande, K., Pascual-Robles, M. A., Nanavati, M., Jahani, M., Cheung, W., Staton, S. E., Muños, S., Nielsen, R., Donovan, L. A., … Rieseberg, L. H. (2020). Massive haplotypes underlie ecotypic differentiation in sunflowers. *Nature*, *584*(7822), 602–607. https://doi.org/10.1038/s41586-020-2467-6

Tulig, M. (2000). *Morphological variation in Mimulus section Diplacus (Scrophulariaceae)*. (Msc), California Polytechnic University.

Turner, T. L., Hahn, M. W., & Nuzhdin, S. V. (2005). Genomic islands of speciation in Anopheles gambiae. *PLoS Biology*, *3*(9), 1572–1578. https://doi.org/10.1371/journal.pbio.0030285

Waayers, G. M. (1996). *Hybridization, introgression, and selection in Mimulus aurantiacus ssp. australis and Mimulus puniceus*. (Msc), San Diego State University.

Wang, Z., Jiang, Y., Yang, X., Bi, H., Li, J., Mao, Y., Ma, Y., Ru, D., Zhang, C., Hao, G., Wang, J., Abbott, R. J., & Liu, J. (2022). Molecular signatures of parallel adaptive divergence causing reproductive isolation and speciation across two genera. *The Innovation*, *3*(3), 100247. https://doi.org/10.1016/j.xinn.2022.100247

Westram, A. M., Faria, R., Johannesson, K., & Butlin, R. (2021). Using replicate hybrid zones to understand the genomic basis of adaptive divergence. *Molecular Ecology*, *30*(15), 3797–3814. https://doi.org/10.1111/mec.15861

Westram, A. M., Rafajlović, M., Chaube, P., Faria, R., Larsson, T., Panova, M., Ravinet, M., Blomberg, A., Mehlig, B., Johannesson, K., & Butlin, R. (2018). Clines on the seashore: The genomic architecture underlying rapid divergence in the face of gene flow. *Evolution Letters*, *2*(4), 297–309. https://doi.org/10.1002/evl3.74

Yeaman, S., & Whitlock, M. C. (2011). The genetic architecture of adaptation under migration-selection balance. *Evolution*, *65*(7), 1897–1911. https://doi.org/10.1111/j.1558-5646.2011.01269.x

SUPPORTING INFORMATION

Additional supporting information can be found online in the Supporting Information section at the end of this article.

How to cite this article: Stankowski, S., Chase, M. A., McIntosh, H., & Streisfeld, M. A. (2023). Integrating top-down and bottom-up approaches to understand the genetic architecture of speciation across a monkeyflower hybrid zone. *Molecular Ecology*, *00*, 1–14. https://doi.org/10.1111/mec.16849